THE JOURNAL OF PHYSICAL CHEMISTRY C

Article

Cite This: J. Phys. Chem. C 2018, 122, 14467−14473

pubs.acs.org/JPCC

Achieving High-Performance Surface-Enhanced Raman Scattering through One-Step Thermal Treatment of Bulk MoS_2

Dandan Yan,[†] Wu Qiu,[‡] Xuejiao Chen,[§] Lei Liu,[§] Yongjue Lai,[†] Zhaohui Meng,[†] Jiepeng Song,[†] Yufei Liu,[∥] Xiang-Yang Liu,*[,†,‡,⊥] and Da Zhan*[,†]

[†]Research Institute for Soft Matter and Biomimetics, College of Materials, and [‡]Department of Physics, Xiamen University, Xiamen, Fujian 361005, China

[§]Changchun Institute of Optics, Fine Mechanics and Physics, Chinese Academy of Sciences, Changchun, Jilin 130000, China

[∥]Key Laboratory of Optoelectronic Technology & Systems (Chongqing University), Ministry of Education, Chongqing 400044, China

[⊥]Department of Physics, National University of Singapore, 2 Science Drive 3, Singapore 117542, Singapore

Supporting Information

ABSTRACT: We present a strong Raman enhancement substrate through one-step thermal treatment of bulk MoS_2. The substrate provides very efficient hot spots by using the rhodamine 6G (R6G) molecule as a probe. Raman and photoluminescence spectra of modified MoS_2 reveal the detailed mechanism for enhancing Raman signal of R6G. It is found that both the substrate roughness and the slight chemical bond broken on the surface are the main driven forces to induce the surface enhanced Raman scattering (SERS) effects. The minimum detectable concentration of R6G on the most optimized thermally treated MoS_2 can be as low as 10^{-8} M. This synthetic approach is facile, sensitive, and reliable, which shows great potential to be an excellent SERS substrate for biological and chemical detection.

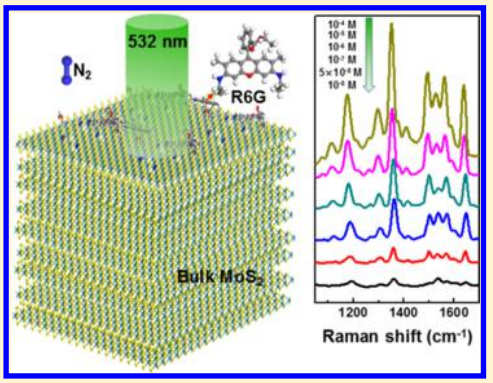

1. INTRODUCTION

Graphene has attracted enormous attention because of its outstanding electronic,[1] optical,[2] and mechanical[3] properties. However, the application of graphene has been greatly restricted in nanoelectronics fields because of the lack of band gap. Meanwhile, other two-dimensional (2D) materials with a natural intrinsic band gap structure have been extensively studied, of which MoS_2, as a typical transition metal dichalcogenide, is of particular interest to scientific community. In the bulk form, MoS_2 is an indirect band gap semiconductor with a 1.2 eV band gap. On the contrary, single-layer MoS_2 has a 1.9 eV direct band gap, which has been extensively applied in fields such as field-effect transistors,[4] photocatalysis, chemical vapor sensors,[5] and lithium ion batteries,[6] and so forth. Furthermore, it is worth noting that MoS_2 is not limited only by the aforementioned applications. For example, Shen and his co-workers first reported that plasma-modified thin-layer MoS_2 for enhancing rhodamine 6G (R6G) molecules Raman signal intensity, which can be used as an active substrate for surface-enhanced Raman scattering (SERS)[7]. Shen attributed this enhancement effect to the disordered surface structure of MoS_2 and the band filling effect because of the strong electronegativity of the absorbed oxygen.[7] Kong's group reported that almost all the 2D materials thinned down to 1 layer, such as MoS_2, h-BN, and graphene and can be served as the active substrates for enhancing Raman signal in spite of relatively low enhancement effects.[8] Furthermore, Wang et al. reported that the combination of the gold nanoparticle and single-layer MoS_2 can form efficient SERS hot spots with an improved detection sensitivity.[9] However, the side effects such as the reaction between noble metal and adsorbate as well as the strong background spectrum will be formed because of the catalytic and carbonization effects on the noble metal. Furthermore, the expensive price of noble metal is another unavoidable factor that has limited its wide applications in the SERS. To date, the Raman enhancement mechanism for the 2D materials can be summarized in terms of the following viewpoints: (1) local dipole coupling leads to the SERS;[10] (2) charge transfer between substrate and adsorbate;[5] (3) the nanocomposite of 2D materials with a high surface area combining with noble metal exhibits synergistic effects as an effective SERS substrate.[11]

Despite the fact that so many SERS papers[7−9,11−16] have been reported based on 2D materials, most of them are focused on the thin-layer or hybrid structure. In this work, we designed a new kind of SERS substrate referred to as a one-step thermal-treated bulk MoS_2. It is found that the thermally

Received: February 22, 2018
Revised: April 26, 2018
Published: June 4, 2018

DOI: 10.1021/acs.jpcc.8b01822
J. Phys. Chem. C 2018, 122, 14467−14473

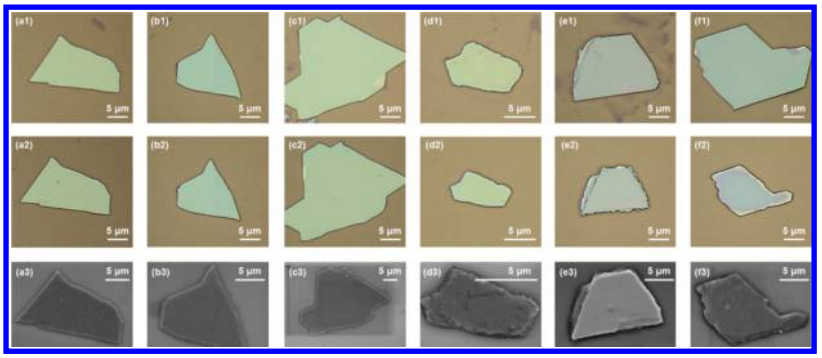

Figure 1. Optical images of mechanically exfoliated bulk MoS_2 before (a1−f1) and after (a2−f2) thermal annealing in ambient air for 1 h at 350 (a2), 375 (b2), 400 (c2), 425 (d2), 450 (e2), and 475 °C (f2), respectively. SEM images for pristine bulk MoS_2 (a3−f3) and thermal annealing in ambient air-treated MoS_2 for 1 h at 350 (a3), 375 (b3), 400 (c3), 425 (d3), 450 (e3), and 475 °C (f3).

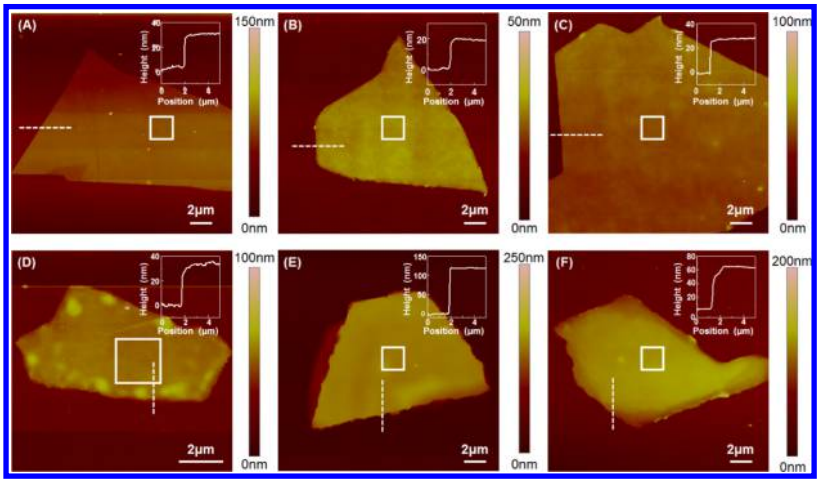

Figure 2. AFM images with the height profile of thermal annealed MoS_2 in ambient air for 1 h at 350 (A), 375 (B), 400 (C), 425 (D), 450 (E), and 475 °C (F), respectively.

modified bulk MoS_2 is an ultrasensitive active substrate for enhancing Raman intensity of R6G molecules. Conventionally, bulk MoS_2 presents a relatively weaker Raman enhancement effect than other 2D materials.[8] However, when the R6G deposited on the one-step thermal-treated bulk MoS_2 surface, the Raman enhancement effect will be dramatically increased compared to that of pristine bulk MoS_2. The enhancement efficiency is even comparable to single-layer graphene and graphene−gold nanoparticle hybrid films.[12,13] This kind of surface-modified MoS_2 is proven to be a very efficient SERS substrate with hot spots by using the dye molecule rhodamine 6G (R6G) molecule as a probe.

2. EXPERIMENTAL SECTION

2.1. Reagents and Materials. Rhodamine 6G (R6G, 95%) was bought from Aladdin. The MoS_2 crystal was provided by SPI. All chemicals were directly used without further purification.

2.2. Apparatus and Measurements. Both micro-Raman and photoluminescence (PL) measurements were carried out by using a Horiba-JobinYvon system with an excitation laser wavelength of 532 nm and 100X objective lens (numerical aperture = 0.95). The laser power is strictly controlled below 0.5 mW to avoid the laser-induced thermal effect on the sample. The size of the focused laser beam is ~1 μm, and the pinhole is 100 for each spectrum. To obtain the optimized comparison of the spectra, all the spectra were collected using the same parameters.

A laser microscope (3D& Profile Measurement KEYENCE, VK-X200 series) was used to locate MoS_2 as well as to capture the samples' optical images.

Atomic force microscopy (AFM, Bruker, Dimension Icon) was used to measure the height profiles and surface morphologies of MoS_2. The scan line is 512 and the scan rate is 0.5 Hz.

Scanning electron microscopy (SEM, Hitachi SU70) was used to observe the morphologies of pristine MoS_2 and the treated MoS_2 surface.

A tube furnace (OTF-1200X) was used for thermal annealing treatment of MoS_2.

Fabrication of pristine MoS_2 and thermal annealing treatment of MoS_2: Pristine bulk MoS_2 was prepared by mechanical exfoliation from a natural MoS_2 crystal (SPI supplied) and was transferred onto a freshly cleaned Si substrate deposited by 300 nm SiO_2. The as-received samples were then thermal-annealed in the air atmosphere, and followed by immersing them in R6G molecule solutions with various concentrations for 2 h.

3. RESULTS AND DISCUSSION

Figure 1 shows the optical images of exfoliated MoS_2 and thermal annealing-treated MoS_2 on the SiO_2/Si substrate. Figure 1a1−f1 show the optical images of various mechanical

DOI: 10.1021/acs.jpcc.8b01822
J. Phys. Chem. C 2018, 122, 14467−14473

exfoliated MoS_2 samples before thermal annealing. The bulk MoS_2 samples with annealing temperature not higher than 425 °C used in this work are of similar thickness as we intentionally selected the samples with very similar optical contrast, and the thickness are all in the range of 20−35 nm as confirmed by AFM (Figure 2A−D). On the other hand, we have chosen much thicker samples to be annealed at 450 and 475 °C, as the samples with the thickness less than 35 nm normally disappeared after annealing at these high temperatures (strong etching effect). It is noteworthy that all the selected samples can present the bulk properties and can fully exclude the substrate electrostatic influence fully as they are thicker than 20 nm.[17] We choose two bulk MoS_2 samples with obvious different thicknesses (thicker than 20 nm) deposited on the same SiO_2/Si substrate and annealed at 375 °C for 1 h, and it can be seen that the SERS effect does not show observable difference (Supporting Information, Figure S1). Then, thermal annealing treatment was performed in ambient air for 1 h at various temperatures (350, 375, 400, 425, 450, and 475 °C), and the corresponding images compared to the pristine images are shown in Figure 1a2−f2.

It is clearly seen that the surfaces of bulk MoS_2 do not present obvious change when the thermal annealing temperatures are 350, 375, and 400 °C (Figure 1a2−c2), though the samples shrink a little bit (note that the sample morphology does not show any observable change by optical microscopy below 350 °C, and thus the lowest annealing temperature 350 °C was chosen in this work). With the thermal annealing temperature continually increased to 425 °C or higher, the shapes of the bulk MoS_2 shrink apparently as shown in Figure 1d2−f2. Because the samples were annealed in ambient air which contains enough O_2/N_2, we may ascribe this shrinking phenomenon to the oxygen or nitrogen etching effect of MoS_2 from edges,[18−21] and we also identify the difference for MoS_2 samples that are thermally annealed in N_2 and O_2, respectively. It is found that annealed MoS_2 in the N_2 atmosphere can be more easily etched than that of the MoS_2 in O_2 for the same annealing temperature (Figure S2A).

It is worth noting that we have tried using 500 °C as the annealing temperature and found that almost all the bulk samples etched out, in this regards, the highest annealing temperature was chosen at 475 °C throughout our experiment. To clearly characterize the etching effect of edges and the surfaces of the thermal annealed samples at various temperatures, the samples were further observed by SEM. The SEM image (Figure S3 in the Supporting Information) of exfoliated pristine bulk MoS_2 shows that the MoS_2 surface is very smooth and the edges are very straight. From Figure 1a3−f3, we can obviously notice that the etching effect of MoS_2 at edges becomes more prominent with the increase of annealing temperature. On the other hand, the surface of annealed samples is not as smooth as the ideal 2D surface that we normally imaged, particularly that the sample annealed at 425 °C seems to have the roughest surface.

For the surface-modified bulk MoS_2 by thermal annealing treatment in ambient air, we surprisingly found that it is an ideal substrate for SERS by using the R6G molecule as a probe compared to the traditional single- or few-layer MoS_2 reported elsewhere,[7,8] and it even performed much better enhancement compared the MoS_2 mediated with gold nanoparticles as a synergetic reaction[9,22−24] (the detailed quantitative SERS analysis will be shown later in this paper). The influence of enhanced Raman intensity for R6G deposited on various substrates is shown in Figure 3A. There is no Raman signal of the R6G molecule when it is directly deposited on the SiO_2/Si

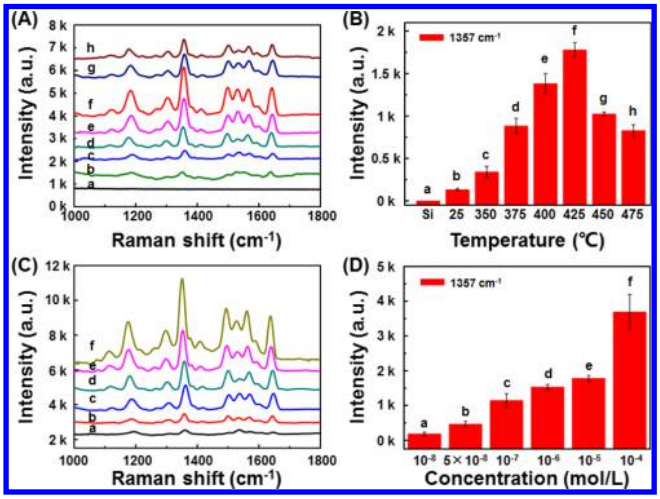

Figure 3. (A) Raman spectra of R6G molecules. (B) Raman intensity (integrated with the peak at ∼1357 cm^{-1}) of R6G molecules deposited on different SERS-active substrates: (a) SiO_2/Si, (b) pristine MoS_2, (c) 350 °C treated MoS_2, (d) 375 °C treated MoS_2, (e) 400 °C treated MoS_2, (f) 425 °C treated MoS_2, (g) 450 °C treated MoS_2, and (h) 475 °C treated MoS_2. (C) Raman spectra of R6G molecules deposited on 425 °C annealed bulk MoS_2 with different concentrations: (a) 10^{-8}, (b) 5×10^{-8}, (c) 10^{-7}, (d) 10^{-6}, (e) 10^{-5}, and (f) 10^{-4} M. (D) Raman intensity (integrated with the peak at ∼1357 cm^{-1}) of R6G deposited on 425 °C annealed bulk MoS_2 at 1357 cm^{-1} for various R6G concentrations.

surface, as shown in Figure 3A(a). When pristine bulk MoS_2 is used as the SERS-active substrate, the detected R6G Raman signals are too weak to be seen as shown by the black curve in Figure 3A. On the contrary, all the annealed samples present feature Raman peaks of R6G molecules (located at 1177, 1357, 1495, 1530, 1563, and 1639 cm^{-1}) because of the SERS effects.[11,25] For the annealed samples, it is found that the Raman intensity of R6G molecules varies regularly with the thermal annealing temperature. The SERS effect increases with the annealing temperature up to 425 °C. Then, it is noted that the SERS effect decreases gradually with the annealing temperature higher than 425 °C. AFM measurement was carried out to see the modification of the structure of the surface (Figure 2). It is also found that the roughness of the MoS_2 surface does not show obvious changes except for the sample that annealed at 425 °C which shows a relatively larger root mean square roughness (rms roughness) value (Figure 4A). Previously, the reported Raman enhancement mechanisms are closely related to the electrical properties and chemical bonds of the material-based substrate. In our experiment, though the main etching in ambient air occurs at the edges of bulk MoS_2 during the annealing process, the ambient air etching-induced damage for the surface molecular structure is also inevitable, particularly when the sample annealed at 425 °C presents much more obvious surface modification in the microstructure (Figures 1d3 and 2B). It is worth noting that the annealing temperature-dependent SERS effect is reproducible, as we measured more than 80 samples totally. In terms of the previous reported SERS for 2D materials, the annealing normally gives rise to two main features for SERS: (1), removing the surface contaminants to effectively enhance the direct contact between the surface and

DOI: 10.1021/acs.jpcc.8b01822
J. Phys. Chem. C 2018, 122, 14467−14473

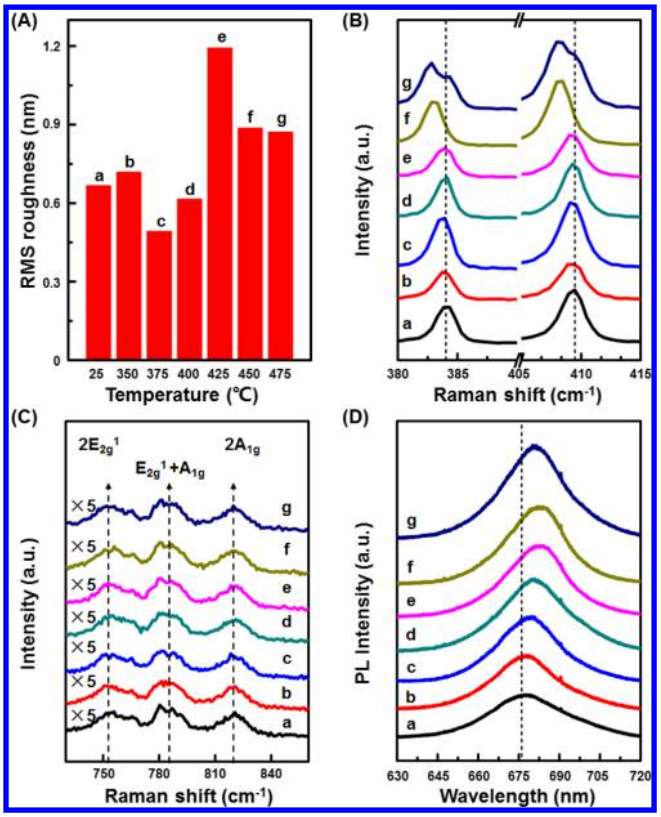

Figure 4. (A) RMS value of bulk MoS_2 as a function of the annealing temperature. The RMS value is measured in terms of the region marked by a white square in each image of Figure 2B Raman spectra for pristine and thermal annealing treated-MoS_2 samples. (C) Raman spectra in the range of 730−860 cm^{-1}. (D) PL spectra for pristine and thermal annealing treated MoS_2 samples. (a) Pristine MoS_2, (b) 350 °C treated MoS_2, (c) 375 °C treated MoS_2, (d) 400 °C treated MoS_2, (e) 425 °C treated MoS_2, (f) 450 °C treated MoS_2, and (g) 475 °C treated MoS_2.

R6G molecules;[14,26] (2) the surface structural disorder can create local dipole as well as make the adsorption of O_2/N_2 much stronger, giving rise to the symmetry breaking of the contacted R6G molecules as well as the strong charge transfer to finally realize SERS. Therefore, we further carried out the Raman and PL measurements to analyze the corresponding surface doping effect of MoS_2, which will be shown in detail later.

The 425 °C thermal annealing treated MoS_2 substrate presents the best SERS effect for detecting R6G molecules; therefore, we further studied the SERS performance on molecular detecting sensitivity using this specified substrate. The enhanced Raman spectra of R6G with various concentrations deposited on 425 °C thermal annealing treated bulk MoS_2 substrates are shown in Figure 3C. The R6G Raman modes present very prominent signals for the high concentration sample (10^{-4} M). The Raman signals decrease slowly with the decreasing concentration of R6G down to 1×10^{-7} M, and the peaks for the 5×10^{-8} M sample dropped dramatically but can be observed clearly. To approach the bottom limit, we found that even for the sample with the concentration as low as 1×10^{-8} M, the Raman signal can still be activated successfully, though the peaks are very weak (a curve in Figure 3Ca). To quantitatively illustrate the SERS effect, Figure 3D gives the integrated Raman peak intensity for the mode at 1357 cm^{-1} as a function of the concentration of the R6G molecule. It is clearly seen that for the concentration of 1×10^{-8} M, the peak intensity decreases to more than one order lower compared to that of the 10^{-4} M sample. The detection of the minimum concentration of R6G as low as 1×10^{-8} M demonstrates that the thermally treated bulk MoS_2 at the temperature of 425 °C has the most sensitivity as an active SERS substrate compared to other MoS_2-based materials as reported elsewhere,[7,9,27] and the enhancing effect is even comparable to single-layer graphene and graphene−Au/Ag nanoparticle[28] hybrid structure.[12,13,29,30] The enhancement factor is found to be $\sim 1.9 \times 10^6$, and the detailed calculation method can be found in the Supporting Information.

The formation of structural disorder due to the molecular damage at the surface can give rise to the creation of the local dipole, which is the driven force for the molecular symmetry breaking-induced SERS effect. Meanwhile, the formation of structural disorder can be the center for adsorbing O_2/N_2 from the environment. In the previous work, it is found that the O_2 and N_2 would give rise to p-doping and n-doping to MoS_2, respectively, because of the strong/weak electron negativity of adsorbed O_2/N_2.[7,19,31,32] Raman spectroscopy is proved to be a very powerful scientific tool to study the detailed physical and chemical properties of 2D materials, particularly for graphene[20,33] and MoS_2.[19,21,34−36] For the Raman spectra of pristine and thermal annealing treated MoS_2 samples (Figure 4B), as can be seen, the thermal annealing treatments do not shift both E^1_{2g} (384 cm^{-1}) and A_{1g} (408 cm^{-1}) modes for annealing temperatures not higher than 400 °C. It is also found that the linewidths for both E^1_{2g} (~1.9 cm^{-1}) and A_{1g} (~2.4 cm^{-1}) modes of these samples keep unchanged after thermal annealing treatment, as shown in Figure 4B, which indicates that the main crystal structure of MoS_2 at the center area of each sample does not change, though they experienced the thermal treatment even in ambient air. The crystalline quality of the precursor MoS_2 crystal is extremely good as indicated by X-ray diffraction (XRD) (Figure S4). This is also an evidence to show that the bulk MoS_2 is relatively thermally stable in air, and the air-induced etching effect mainly occurs at the edges, as the crystal structure at edges is not perfect and it can be considered as the defect region, which is much more vulnerable to air at high temperature.[37] When the sample annealed at 425 °C, the E^1_{2g} mode is still kept at the original position, but the A_{1g} mode shows a red shift slightly. Traditionally, the A_{1g} mode can be blue-shifted/red-shifted, while the E^1_{2g} mode is unaffected for the O_2/N_2 physically adsorbed single- and few-layer MoS_2 because of the change of electron−phonon interactions,[7,19] of which the phenomenon is very similar to that of the 425 °C annealed sample. Now, we can confirm that the surface adsorption is mainly dominated by N_2, as it gives rise to the electron doping of MoS_2;[7,31,32] as a consequence, the A_{1g} mode shifted to lower frequency. When the annealing temperature continuously increases to even higher temperatures of 450 and 475 °C, it is found that both the E^1_{2g} and A_{1g} modes show dramatic red shift. It is obvious that both Raman modes split into two subpeaks for the 475 °C annealed sample, indicating the extremely strong doping with introducing a large amount of defects.[38] Furthermore, as shown in Figure 4C, the Raman spectra of the annealed bulk MoS_2 samples in the range of 730−860 cm^{-1} only present three observed modes of MoS_2, which are $2E^1_{2g}$, $E^1_{2g} + A_{1g}$, and $2A_{1g}$,[39] illustrating that the thermally treated MoS_2 samples have not been oxidized to form the MoO_3 crystal phase.[40]

DOI: 10.1021/acs.jpcc.8b01822
J. Phys. Chem. C 2018, 122, 14467−14473

Apart from Raman spectroscopy, PL spectroscopy has also been extensively studied in determining the doping level of MoS_2.[19,41] To explain the mechanism of Raman enhancement for thermal annealing treated bulk MoS_2, we further carried out the PL measurements of pristine MoS_2 and thermally treated MoS_2, as shown in Figure 4C. The red-shift phenomenon of PL peak wavelength (A-exciton) is observed for all the annealed samples compared to that of the pristine bulk sample. The red shift of PL is mainly ascribed to the electron doping-induced upshift of the Fermi level, which is in accordance with the Raman results. The shifted frequency of the peak position increases with the annealing temperature and reaches the maximum at 425 °C, and then the red-shifted frequency decreases gradually with the increasing annealing temperature up to 475 °C. To further confirm that the red-shift phenomena for both Raman and PL of annealed MoS_2 are caused by the adsorption of N_2 from ambient air,[37] we carried out density functional theory[42,43] to get the band structures of MoS_2, which are performed by using the VASP package, and the core electrons are treated with the projector-augmented wave method.[44,45] The band structures are calculated along the high symmetry point without spin−orbit coupling. The upshift of the Fermi level with nitrogen-doped MoS_2 was found (Figure 5B) and compared to that with the pristine MoS_2 (Figure 5A). It is suggested that the electron negativity of nitrogen is weaker compared to that of MoS_2 and thus gives rise to the N-doping effect to MoS_2. Therefore, it is theoretically explained the red-shift phenomena of both Raman frequency and PL wavelength are indeed caused by the nitrogen-doping effect as mentioned before.[31] We also carried out the experiments on annealing two bulk MoS_2 in N_2 and O_2, respectively, and the detailed analysis based on PL and Raman spectra also supported our viewpoint very well (see the Supporting Information). It is worth noting that the SERS of MoS_2 is not only limited by nitrogen doping, and very recently, Zhao and his co-workers also have successfully synthesized a sensitive MoS_2-based SERS substrate by oxygen incorporation.[16]

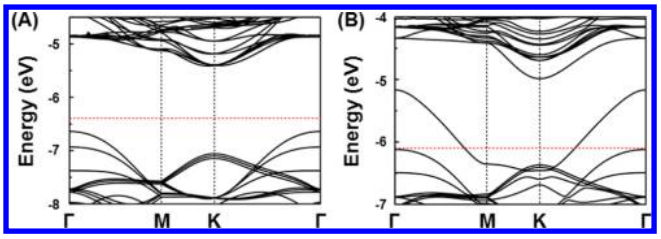

Figure 5. Band structures of (A) pristine MoS_2 and (B) nitrogen doping case. The red line is the Fermi energy level. The zero point is the vacuum point.

Moreover, PL spectra of thermally treated MoS_2 by depositing R6G are also analyzed. Compared to the PL peak that red-shifted to higher wavelength for each annealed sample as mentioned above, it is found that each sample's PL peak position underwent a blue shift after depositing R6G (Figure 6). The blue-shift phenomenon is mainly owing to the charge transfer effect[27,46] between R6G and thermally treated MoS_2. The symmetry of R6G molecules are unavoidably to be broken because of the charge transfer reaction, and as a consequence, giving rise to the activation of its Raman modes which are inactive originally. It is obviously seen that compared to other thermal annealed samples, the 425 °C annealed sample has undergone the most blue shift (Figure 6D) compared to other annealed samples, indicating the most effective charge transfer in this specified sample. Therefore, the previously revealed maximum SERS effect by using 425 °C thermally annealed bulk MoS_2 sample can be well explained, of which the most deposited R6G molecules underwent a very efficient symmetry breaking because of the strongest charge transfer reaction, leading to the best SERS effect compared to other samples. Furthermore, it is worth noting that for the samples that underwent an even higher temperature annealing process (450 and 475 °C), the SERS effect is weaker compared to that of the 425 °C annealed sample. We can combine both Raman and PL results to explain this phenomenon. The Raman results illustrate that the MoS_2 has been doped by electrons (N-doping by nitrogen) effectively while it kept its crystallinity as well for the 425 °C annealed sample, as it shows a phenomenon similar to the results reported elsewhere.[7,19,47] Despite the fact that obvious frequency shift for both E^1_{2g} and A_{1g} modes indicate the extremely strong electron doping effect for the highest annealing temperature (475 °C), however, the splitting of the peaks (Figure 4B-g) is the direct evidence to show the appearance of a large amount of defects, which means that the crystallinity of MoS_2 has been damaged to some

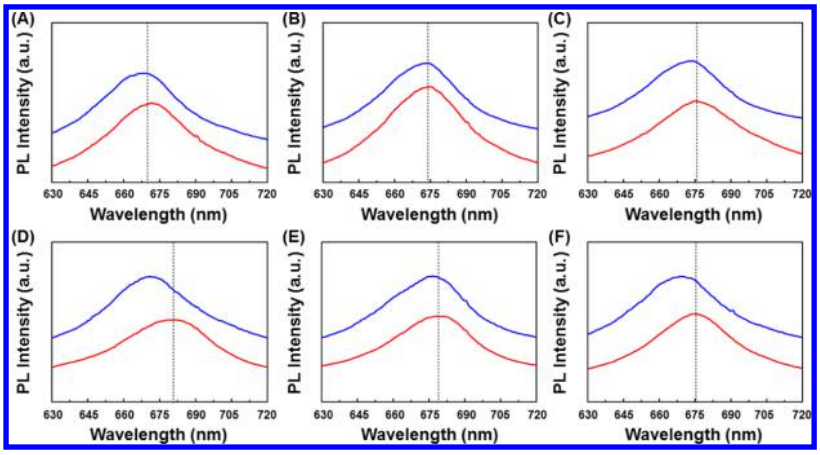

Figure 6. PL spectra for the bulk MoS_2 samples: (A) 350 °C treated MoS_2, (B) 375 °C treated MoS_2, (C) 400 °C treated MoS_2, (D) 425 °C treated MoS_2, (E) 450 °C treated MoS_2, and (F) 475 °C treated MoS_2. The red curves represent PL spectra for MoS_2 after thermal annealing treatment at various temperatures, and blue curves are the corresponding PL spectra of MoS_2 with deposition of R6G.

DOI: 10.1021/acs.jpcc.8b01822
J. Phys. Chem. C 2018, 122, 14467−14473

extent. Therefore, it is probably the reason why the red-shifted wavelength of PL is also smaller compared to that of the 425 °C annealed sample, and consequently, the interaction of charge transfer with R6G is also relatively weaker, giving rise to the lower SERS effect.

4. CONCLUSIONS

To summarize, an efficient Raman-active bulk MoS_2 is successfully fabricated by the thermal annealing process. It is experimentally and theoretically revealed that annealing in ambient air would modify the surface structure properly and introduce the effective N-doping effect to the bulk MoS_2, leading it to be an active SERS substrate. The SERS effect of the annealed bulk MoS_2 is associated with the annealing temperature obviously. The mechanism of annealing temperature-dependent SERS effect is analyzed in detail using Raman and PL spectroscopies. It is found that 425 °C is the critical temperature that can give the most surface structural disorder but still keep its crystallinity by the detailed analysis using Raman and PL spectroscopies, and thus 425 °C thermal annealed MoS_2 substrate possesses the most optimized sensitivity, which also performs much better compared to other MoS_2-based SERS substrates as reported previously. This work is on the basis of facile and convenient, in addition, as bulk MoS_2 is naturally existed widely, the amplification of SERS effect by using the simply modified bulk MoS_2 can be well applied for chemical and biological molecules detection in future, indicating a new way to expand the applications of using bulk MoS_2 through surface engineering.

■ ASSOCIATED CONTENT

Supporting Information

The Supporting Information is available free of charge on the ACS Publications website at DOI: 10.1021/acs.jpcc.8b01822.

Raman spectra of R6G molecules deposited onto two bulk MoS_2 with different thickness; optical images, PL spectra and Raman spectra of bulk MoS_2 before and after annealing in N_2 and O_2, respectively; SEM image of pristine bulk MoS_2; XRD analysis for bulk MoS_2; and enhancement factor calculation (PDF)

■ AUTHOR INFORMATION

Corresponding Authors

*E-mail: phyliuxy@nus.edu.sg (X.-Y.L.).
*E-mail: zhanda@xmu.edu.cn (D.Z.).

ORCID

Da Zhan: 0000-0001-5270-936X

Notes

The authors declare no competing financial interest.

■ ACKNOWLEDGMENTS

The work in Xiamen University was supported by NSFC (grant no. 11404272), the Fundamental Research Funds for the Central Universities (grant no. 20720140514), the Natural Science Foundation of Fujian Province of China (grant no. 22171024), the Undergraduate Innovation and Entrepreneurship Training Programs (grant no. 2015X2011), the Doctoral Fund of the Ministry (grant no. 20130121110018), and Huazhou Institute of Novel Materials of Xiamen University. The work in CAS was supported by National Science Fund for Distinguished Young Scholars of China (no. 61525404). The work in Chongqing University was supported by the National Key Research and Development Program of China (grant no. 2016YFC0101100 and 2016YFE0125200). The authors acknowledge Xiuming Zhang (optical measurement), Yange Wang (SEM analysis), and Rui Yu (AFM analysis) for their technical help in experiments.

■ REFERENCES

(1) Novoselov, K. S.; Geim, A. K.; Morozov, S. V.; Jiang, D.; Katsnelson, M. I.; Grigorieva, I. V.; Dubonos, S. V.; Firsov, A. A. Two-Dimensional Gas of Massless Dirac Fermions in Graphene. *Nature* **2005**, *438*, 197−200.

(2) Bao, Q.; Zhang, H.; Wang, B.; Ni, Z.; Lim, C. H. Y. X.; Wang, Y.; Tang, D. Y.; Loh, K. P. Broadband Graphene Polarizer. *Nat. Photonics* **2011**, *5*, 411−415.

(3) Lee, C.; Wei, X.; Kysar, J. W.; Hone, J. Measurement of the Elastic Properties and Intrinsic Strength of Monolayer Graphene. *Science* **2008**, *321*, 385−388.

(4) Radisavljevic, B.; Radenovic, A.; Brivio, J.; Giacometti, V.; Kis, A. Single-layer MoS2 transistors. *Nat. Nanotechnol.* **2011**, *6*, 147−150.

(5) Perkins, F. K.; Friedman, A. L.; Cobas, E.; Campbell, P. M.; Jernigan, G. G.; Jonker, B. T. Chemical Vapor Sensing with Monolayer MoS2. *Nano Lett.* **2013**, *13*, 668−673.

(6) Hwang, H.; Kim, H.; Cho, J. MoS2Nanoplates Consisting of Disordered Graphene-like Layers for High Rate Lithium Battery Anode Materials. *Nano Lett.* **2011**, *11*, 4826−4830.

(7) Sun, L.; Hu, H.; Zhan, D.; Yan, J.; Liu, L.; Teguh, J. S.; Yeow, E. K. L.; Lee, P. S.; Shen, Z. Plasma Modified MoS2Nanoflakes for Surface Enhanced Raman Scattering. *Small* **2014**, *10*, 1090−1095.

(8) Ling, X.; Fang, W.; Lee, Y.-H.; Araujo, P. T.; Zhang, X.; Rodriguez-Nieva, J. F.; Lin, Y.; Zhang, J.; Kong, J.; Dresselhaus, M. S. Raman Enhancement Effect on Two-Dimensional Layered Materials: Graphene, H-BN and MoS2. *Nano Lett.* **2014**, *14*, 3033−3040.

(9) Su, S.; Zhang, C.; Yuwen, L.; Chao, J.; Zuo, X.; Liu, X.; Song, C.; Fan, C.; Wang, L. Creating SERS Hot Spots on MoS2 Nanosheets with in Situ Grown Gold Nanoparticles. *ACS Appl. Mater. Interfaces* **2014**, *6*, 18735−18741.

(10) Yu, X.; Lin, K.; Qiu, K.; Cai, H.; Li, X.; Liu, J.; Pan, N.; Fu, S.; Luo, Y.; Wang, X. Increased Chemical Enhancement of Raman Spectra for Molecules Adsorbed on Fluorinated Reduced Graphene Oxide. *Carbon* **2012**, *50*, 4512−4517.

(11) Li, Z.; Jiang, S.; Xu, S.; Zhang, C.; Qiu, H.; Li, C.; Sheng, Y.; Huo, Y.; Yang, C.; Man, B. Few-layer MoS 2 -encapsulated Cu nanoparticle hybrids fabricated by two-step annealing process for surface enhanced Raman scattering. *Sens. Actuators, B* **2016**, *230*, 645−652.

(12) Du, Y.; Zhao, Y.; Qu, Y.; Chen, C.-H.; Chen, C.-M.; Chuang, C.-H.; Zhu, Y. Enhanced light-matter interaction of graphene-gold nanoparticle hybrid films for high-performance SERS detection. *J. Mater. Chem. C* **2014**, *2*, 4683−4691.

(13) Ling, X.; Xie, L.; Fang, Y.; Xu, H.; Zhang, H.; Kong, J.; Dresselhaus, M. S.; Zhang, J.; Liu, Z. Can Graphene Be Used as a Substrate for Raman Enhancement? *Nano Lett.* **2010**, *10*, 553−561.

(14) Wang, Y.; Ni, Z.; Hu, H.; Hao, Y.; Wong, C. P.; Yu, T.; Thong, J. T. L.; Shen, Z. X. Gold on Graphene as a Substrate for Surface Enhanced Raman Scattering Study. *Appl. Phys. Lett.* **2010**, *97*, 163111.

(15) Zheng, J.; Dai, Z.; Mei, F.; Xiao, X.; Liao, L.; Wu, W.; Zhao, X.; Ying, J.; Ren, F.; Jiang, C. Micro-Nanosized Nontraditional Evaporated Structures Based on Closely Packed Monolayer Binary Colloidal Crystals and Their Fine Structure Enhanced Properties. *J. Phys. Chem. C* **2014**, *118*, 20521−20528.

(16) Zheng, Z.; Cong, S.; Gong, W.; Xuan, J.; Li, G.; Lu, W.; Geng, F.; Zhao, Z. Semiconductor SERS Enhancement Enabled by Oxygen Incorporation. *Nat. Commun.* **2017**, *8*, 1993.

(17) Castellanos-Gomez, A.; Cappelluti, E.; Roldán, R.; Agraït, N.; Guinea, F.; Rubio-Bollinger, G. Electric-Field Screening in Atomically Thin Layers of MoS2: the Role of Interlayer Coupling. *Adv. Mater.* **2013**, *25*, 899−903.

DOI: 10.1021/acs.jpcc.8b01822
J. Phys. Chem. C 2018, 122, 14467−14473

(18) Chow, W. L.; Luo, X.; Quek, S. Q.; Tay, B. K. Evolution of Raman Scattering and Electronic Structure of Ultrathin Molybdenum Disulfide by Oxygen Chemisorption. *Adv. Electron. Mater.* **2015**, *1*, 1400037.
(19) Nan, H.; Wang, Z.; Wang, W.; Liang, Z.; Lu, Y.; Chen, Q.; He, D.; Tan, P.; Miao, F.; Wang, X.; Wang, J.; Ni, Z. Strong Photoluminescence Enhancement of MoS2 through Defect Engineering and Oxygen Bonding. *ACS Nano* **2014**, *8*, 5738−5745.
(20) Xu, Y. N.; Zhan, D.; Liu, L.; Suo, H.; Ni, Z. H.; Nguyen, T. T.; Zhao, C.; Shen, Z. X. Thermal Dynamics of Graphene Edges Investigated by Polarized Raman Spectroscopy. *ACS Nano* **2011**, *5*, 147−152.
(21) Zhan, D.; Liu, L.; Xu, Y. N.; Ni, Z. H.; Yan, J. X.; Zhao, C.; Shen, Z. X. Low Temperature Edge Dynamics of AB-Stacked Bilayer Graphene: Naturally Favored Closed Zigzag Edges. *Sci. Rep.* **2011**, *1*, 00012.
(22) Yu, X.; Shiraki, T.; Yang, S.; Ding, B.; Nakashima, N. Synthesis of porous gold nanoparticle/MoS2 nanocomposites based on redox reactions. *RSC Adv.* **2015**, *5*, 86558−86563.
(23) Lu, J.; Lu, J. H.; Liu, H.; Liu, B.; Gong, L.; Tok, E. S.; Loh, K. P.; Sow, C. H. Microlandscaping of Au Nanoparticles on Few-Layer MoS2Films for Chemical Sensing. *Small* **2015**, *11*, 1792−1800.
(24) Fang, S.-U.; Hsu, C.-L.; Hsu, T.-C.; Juang, M.-Y.; Liu, Y.-C. Surface Roughness-Correlated SERS Effect on Au Island-Deposited Substrate. *J. Electroanal. Chem.* **2015**, *741*, 127−133.
(25) Nie, S.; Emery, S. R. Probing Single Molecules and Single Nanoparticles by Surface-Enhanced Raman Scattering. *Science* **1997**, *275*, 1102−1106.
(26) Wang, Y.; Ni, Z.; Li, A.; Zafar, Z.; Zhang, Y.; Ni, Z.; Qu, S.; Qiu, T.; Yu, T.; Xiang Shen, Z. Surface Enhanced Raman Scattering of Aged Graphene: Effects of Annealing in Vacuum. *Appl. Phys. Lett.* **2011**, *99*, 233103.
(27) Lee, Y.; Kim, H.; Lee, J.; Yu, S. H.; Hwang, E.; Lee, C.; Ahn, J.-H.; Cho, J. H. Enhanced Raman Scattering of Rhodamine 6G Films on Two-Dimensional Transition Metal Dichalcogenides Correlated to Photoinduced Charge Transfer. *Chem. Mater.* **2016**, *28*, 180−187.
(28) Dai, Z.; Mei, F.; Xiao, X.; Liao, L.; Fu, L.; Wang, J.; Wu, W.; Guo, S.; Zhao, X.; Li, W.; Ren, F.; Jiang, C. "Rings of saturn-like" nanoarrays with high number density of hot spots for surface-enhanced Raman scattering. *Appl. Phys. Lett.* **2014**, *105*, 033515.
(29) Zhang, C.; Jiang, S. Z.; Huo, Y. Y.; Liu, A. H.; Xu, S. C.; Liu, X. Y.; Sun, Z. C.; Xu, Y. Y.; Li, Z.; Man, B. Y. SERS Detection of R6g Based on a Novel Graphene Oxide/Silver Nanoparticles/Silicon Pyramid Arrays Structure. *Opt. Express* **2015**, *23*, 24811−24821.
(30) Zhang, C.; Li, C.; Yu, J.; Jiang, S.; Xu, S.; Yang, C.; Liu, Y. J.; Gao, X.; Liu, A.; Man, B. SERS Activated Platform with Three-Dimensional Hot Spots and Tunable Nanometer Gap. *Sens. Actuators, B* **2018**, *258*, 163−171.
(31) Liu, W.; Zhao, C.; Zhou, R.; Zhou, D.; Liu, Z.; Lu, X. Lignin-Assisted Exfoliation of Molybdenum Disulfide in Aqueous Media and Its Application in Lithium Ion Batteries. *Nanoscale* **2015**, *7*, 9919−9926.
(32) Singh, A. K.; Andleeb, S.; Singh, J.; Eom, J. Tailoring the electrical properties of multilayer MoS2 transistors using ultraviolet light irradiation. *RSC Adv.* **2015**, *5*, 77014−77018.
(33) Zhan, D.; Yan, J. X.; Ni, Z. H.; Sun, L.; Lai, L. F.; Liu, L.; Liu, X. Y.; Shen, Z. X. Bandgap-Opened Bilayer Graphene Approached by Asymmetrical Intercalation of Trilayer Graphene. *Small* **2015**, *11*, 1177−1182.
(34) Lee, C.; Yan, H.; Brus, L. E.; Heinz, T. F.; Hone, J.; Ryu, S. Anomalous Lattice Vibrations of Single- and Few-Layer MoS2. *ACS Nano* **2010**, *4*, 2695−2700.
(35) Mathew, S.; Gopinadhan, K.; Chan, T. K.; Yu, X. J.; Zhan, D.; Cao, L.; Rusydi, A.; Breese, M. B. H.; Dhar, S.; Shen, Z. X.; Venkatesan, T.; Thong, J. T. L. Magnetism in MoS2 induced by proton irradiation. *Appl. Phys. Lett.* **2012**, *101*, 102103.
(36) Sun, L.; Yan, J.; Zhan, D.; Liu, L.; Hu, H.; Li, H.; Tay, B. K.; Kuo, J.-L.; Huang, C.-C.; Hewak, D. W.; Lee, P. S.; Shen, Z. X. Spin-Orbit Splitting in Single-Layer MoS_2 Revealed by Triply Resonant Raman Scattering. *Phys. Rev. Lett.* **2013**, *111*, 126801.
(37) Li, H.; Huang, M.; Cao, G. Markedly different adsorption behaviors of gas molecules on defective monolayer MoS2: a first-principles study. *Phys. Chem. Chem. Phys.* **2016**, *18*, 15110−15117.
(38) Liu, Y.; Nan, H.; Wu, X.; Pan, W.; Wang, W.; Bai, J.; Zhao, W.; Sun, L.; Wang, X.; Ni, Z. Layer-by-Layer Thinning of MoS2 by Plasma. *ACS Nano* **2013**, *7*, 4202−4209.
(39) Sun, L.; Yan, J.; Zhan, D.; Liu, L.; Hu, H.; Li, H.; Tay, B. K.; Kuo, J.-L.; Huang, C.-C.; Hewak, D. K.; Lee, P. S.; Shen, Z. X. Spin-Orbit Splitting in Single-Layer MoS_2 Revealed by Triply Resonant Raman Scattering. *Phys. Rev. Lett.* **2013**, *111*, 126801.
(40) Haro-Poniatowski, E.; Jouanne, M.; Morhange, J. F.; Julien, C.; Diamant, R.; Fernández-Guasti, M.; Fuentes, G. A.; Alonso, J. C. Micro-Raman characterization of WO3 and MoO3 thin films obtained by pulsed laser irradiation. *Appl. Surf. Sci.* **1998**, *127-129*, 674−678.
(41) Mouri, S.; Miyauchi, Y.; Matsuda, K. Tunable Photoluminescence of Monolayer MoS2 via Chemical Doping. *Nano Lett.* **2013**, *13*, 5944−5948.
(42) Kresse, G.; Furthmüller, J. Efficient iterative schemes forab initiototal-energy calculations using a plane-wave basis set. *Phys. Rev. B: Condens. Matter Mater. Phys.* **1996**, *54*, 11169−11186.
(43) Kresse, G.; Hafner, J. Ab initiomolecular dynamics for liquid metals. *Phys. Rev. B: Condens. Matter Mater. Phys.* **1993**, *47*, 558−561.
(44) Blöchl, P. E. Projector Augmented-Wave Method. *Phys. Rev. B: Condens. Matter Mater. Phys.* **1994**, *50*, 17953−17979.
(45) Kresse, G.; Joubert, D. From Ultrasoft Pseudopotentials to the Projector Augmented-Wave Method. *Phys. Rev. B: Condens. Matter Mater. Phys.* **1999**, *59*, 1758−1775.
(46) Muehlethaler, C.; Considine, C. R.; Menon, V.; Lin, W.-C.; Lee, Y.-H.; Lombardi, J. R. Ultrahigh Raman Enhancement on Monolayer MoS2. *ACS Photonics* **2016**, *3*, 1164−1169.
(47) Wu, J.; Li, H.; Yin, Z.; Li, H.; Liu, J.; Cao, X.; Zhang, Q.; Zhang, H. Layer Thinning and Etching of Mechanically Exfoliated MoS_2 Nanosheets by Thermal Annealing in Air. *Small* **2013**, *9*, 3314−3319.

DOI: 10.1021/acs.jpcc.8b01822
J. Phys. Chem. C 2018, 122, 14467−14473